Experimental study on scour and erosion of blocked dam

Jing ZHANG, Zhi-xue GUO, Shu-you CAO, Feng-guang YANG*

*State Key Laboratory of Hydraulics and Mountain River Engineering, Sichuan University,
Chengdu 610065, P. R. China*

Abstract: This paper presents new experimental data of the erosion rate and sediment transport rate during the processes of dam break caused by overtopping. In order to study the headcut migration, the erosion coefficient was calculated and its peak value was determined near the downstream edge of the dam crest. Then the characteristics of vertical erosion during dam break processes were analyzed by dividing the dam into three regions: the upstream region, middle region, and downstream region. The three regions show different features during headcut migration, but all are exposed to the most intense erosion at the third stage of the dam break process. Finally, three relevant parameters affecting sediment transport were discussed: the length of the dam crest, the inner slope, and the dam composition. The results show that a longer dam crest and flatter inner slope reduce the peak sediment transport rate and prolong the arrival time of peak sediment transport rate; and with the increase of the non-uniformity coefficient S, the peak sediment transport rate initially increases, and then decreases.

Key words: dam break; overtopping; headcut migration; sediment transport

1 Introduction

Dam break results in significant damage to downstream economies and loss of life. For example, the major dam failure event in Diexi Lake, China, in 1933, killed at least 2 423 people (Li et al. 1986). Dam blockages caused by geo-hazards such as landslides, collapse, or debris flow are widespread in mountainous regions, especially after an earthquake. Due to quick deposition, blocked dams consisting of non-cohesive materials always have weak structures, raising possibility of dam break. Schuster and Costa (1986) reported that half of the landslide dams failed within ten days based on 63 cases from literatures. The erosion potential of blocked dams resulting from overtopping during a torrential rain is an important aspect for assessment of structure stability and safety. The simulated results of the breaching process can be used as an upstream boundary condition for flood evolution models, which can be employed for downstream hazard mitigation, contingency evacuation planning, and management decisions.

Dam break problems have drawn a significant amount of attention from governments and researchers from all over the world since the 19th century. Early studies on dam break conducted from the 1890s to 1980s focused on the dam-break flood evolution using a board as a dam to conceptualize the dam break progress (Li and Li 2009). From the 1980s on, researchers realized that the breaching process plays an important role in accurate simulation of flood evolution involving complex water-sediment interaction. In order to understand the breaching process of a dam due to overtopping, numerous physical models have been conducted. For dams made of cohesive materials, the breach erosion processes involving headcut migration and structural failures were studied, and the damage was estimated (Ralston 1987; Dodge 1988). For dams made of non-cohesive materials, Chinnarasri et al. (2003) performed a series of experiments to acquire descriptive conclusions of the flow patterns and damage of dam overtopping. Based on the analysis from previous experiments and observation data, various mathematical models for the breaching process were proposed and widely employed to simulate the dam breaching process and consequent hazards (Zhu 2006; Clayton and Knox 2008; Dumbser 2011). However, few studies about blocked dams were conducted. Only recently, Dai et al. (2005) investigated the landslide dam and subsequent dam-break flood on the Dadu River. Yan et al. (2009) performed an experimental study of the inundation and landslide dam-break flooding over an erodible bed in open channels. Li et al. (2011) integrated the BREACH model and FLO-2D model to simulate the landslide dam breach and provided quantitative information of the debris flow caused by a dam break. Dong et al. (2011) utilized the logistic regression method and the jack-knife technique to predict the failure probability of a landslide dam. Despite many efforts over the past decades to understand the breaching process, it remains unclear due to complex water-sediment interaction and a lack of measured data on the erosion process for dam break.

Headcut retreat, a headward erosion migrating upstream, occurring in rill erosion, gully formation, and arid rangelands, has been widely studied in the past via experimental study, survey investigation, and GIS techniques (Menéndez-Duarte et al. 2007; Marzolff and Poesen 2009; Stavi et al. 2010). Begin et al. (1980) derived the channel bed evolution equation in the form of an error function. Chen and Chen (2006) investigated the migration behavior of retrogressive erosion and the longitudinal profile evolution of a channel consisting of non-cohesive material. Regarding the dam break process, Wahl (1998) argued that headcut migration was a major factor contributing to the development of breaches in earth dams and brought up a promising theory, the theory of headcut erosion, for clay dikes. Wahl (1998) concluded that the stress force caused by a flow vortex attacked the vertical headcut boundary, and then the headcut migrated upstream continually. In fact, headcut migration was observed during the breaching process in non-cohesive materials (Visser 1998). Therefore, research on headcut can provide a strong foundation for studies of the breaching process.

Nevertheless, in-depth knowledge of and data on the mechanisms of dam break are still lacking, let alone blocked dams. This study performed preliminary research on the characteristics of erosion processes for homogeneous blocked dams resulting from overtopping and provided corresponding experimental data and analysis. Physically, large grains such as gravel, cobble, and even boulders are essential components of blocked dam materials and account for a considerable portion. In view of that, the median diameter of the natural non-cohesive sediment used to construct the dam in this study was larger than 1 mm.

2 Experiments and dam break processes

Thirteen dam break experiments were carried out in a 20 m long, 0.5 m wide, and 0.5 m high tilting flume at the State Key Laboratory of Hydraulics and Mountain River Engineering (SKLH) of Sichuan University. The setup was previously constructed by Zhang et al. (2010). Here, the authors only describe it briefly. A limnimeter with an accuracy of 1 mm was installed in the reservoir to continuously measure the water level upstream of the dam. All the experiments were performed with a fixed inflow discharge of 0.54 L/s calibrated with the volume method. The process of breach growth was videotaped with two digital video cameras (one was placed at one side of the flume and the other was above the initial breach of the dam). A 5 cm × 5 cm grid was applied on the glass side wall of the flume. The definition sketch of the initial dam and schematic diagram of the experimental setup can be found in the authors' previous research (Zhang et al. 2010).

The overflow discharge process can be determined by calculating the water volume lost in the reservoir upstream, and has been discussed in detail (Zhang et al. 2010). This paper focuses on data of erosion characteristics and sediment transport. The experimental values of the breach width and elevation in every section were obtained from analysis of the video frames, and both digital video cameras took 25 pictures per second. The analysis of the pictures allowed the calculation of the erosion rate and the sediment transport rate of blocked dams.

Table 1 shows the characteristics of parameters involved in the experiments. The inner slope is defined as the downstream slope of a dam and, correspondingly, the outer slope is the upstream slope (Fig. 1). The non-uniformity coefficient S is defined as $\sqrt{d_{75}/d_{25}}$, where d_{75}

Table 1 Characteristics of parameters involved

Run	θ (°)	S	L (cm)	Run	θ (°)	S	L (cm)
1	21.81	3.14 (Sediment C)	10	8	21.81	2.30 (Sediment B)	20
2	21.81	3.14 (Sediment C)	20	9	21.81	3.21 (Sediment D)	20
3	21.81	3.14 (Sediment C)	25	10	21.81	2.74 (Sediment E)	20
4	26.58	3.14 (Sediment C)	20	11	21.81	2.80 (Sediment F)	20
5	18.44	3.14 (Sediment C)	20	12	21.81	2.18 (Sediment G)	20
6	14.04	3.14 (Sediment C)	20	13	21.81	2.55 (Sediment H)	20
7	21.81	2.25 (Sediment A)	20				

and d_{25} are the sediment sizes for which 75% and 25% of the particles by weight are finer, respectively. In the thirteen experiments, the outer slope (45°), initial breach elevation (20 cm), and inflow discharge (0.54 L/s) were the same, while the inner slope gradient, the grain size distribution represented by non-uniformity coefficient, and the dam crest length were different. The experimental data set spanned at the angle of the inner slope θ from 14.04° to 26.58°, the coefficient of non-uniformity S from 2.18 to 3.21, and the dam crest length L from 10 cm to 25 cm.
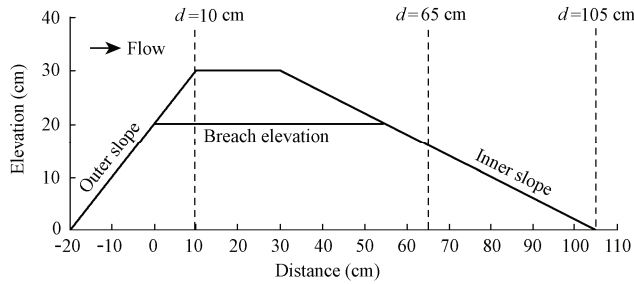
Fig. 1 Sketch of blocked dam

Fig. 2 shows the grain size distributions of eight different sediments with a density of 2 650 kg/m³ used for the dam construction, and they are numbered from sediments A to H. Sediment A is composed of natural fine grains with a sediment particle diameter of $d \leq 10 \text{ mm}$, and natural coarse grains with a sediment particle diameter of $10 \text{ mm} < d \leq 12 \text{ mm}$ are added to it to acquire sediments B to H, depending on the quantity of coarse grains.

During the gradual dam break process, four stages can be distinguished, as follows. In the first and second stages, vertical erosion in the form of a headcut (Fig. 3) is dominant, and only the inner slope is eroded. In the third stage, horizontal erosion is dominant and the erosion is most intense in both the vertical and horizontal directions due to the reduction of breach elevation. During this period, the outer slope suffers the erosion. In the fourth stage, the shape of the dam body remains steady and the reservoir elevation gradually comes to a constant level. The authors described the dam break process in detail and presented a sketch of the evolution of the dam profile over time in a previous study (Zhang et al. 2010).
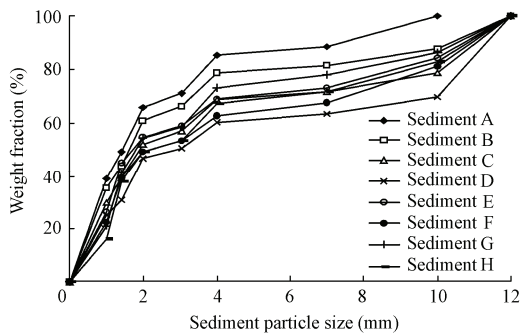

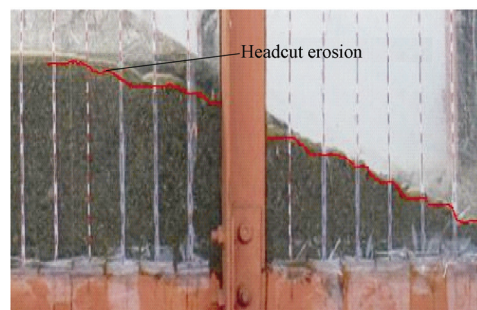**Fig. 2** Grain-size distribution curves

Fig. 3 Longitudinal profile of dam with headcut for run 5

3 Results and discussion

3.1 Erosion rate

After flow overtopping, the headcut started to occur on the inner slope of the dam. During the first two stages, the downstream slope of the headcut was steeper than the upstream slope. Therefore, both the hydraulic force and flow velocity downstream were larger than those upstream, resulting in a high erosion rate downstream and a low erosion rate upstream. As a result, the headcut migrated from the inner slope to the dam crest. Using the equation for headcut evolution derived by Begin et al. (1980), the erosion coefficient can be calculated:

$$\frac{\Delta z}{z_0} = 1 - \mathrm{erf}\left(\frac{x}{At^{0.5}}\right) \tag{1}$$

where Δz is the difference in elevation, z_0 is the base level of the dam, erf (*) is the error function, x is the distance from the point of onset of the erosion occurring on the inner slope, A is the erosion coefficient of the headcut, and t is time.

For Eq. (1), A represents the intensity of the headcut phenomenon, in which A will increase when headcut erosion severely increases, and vice versa. Therefore, study of the variation of the erosion coefficient along the dam profile with elapsed time is crucial to understanding the headcut phase during the dam break process. Fig. 4 shows the variation of the erosion coefficient A along the dam profile during the first two stages of the dam break process. Due to limited drag force provided by overflow, part of the coarse grains deposited on the downstream of the inner slope, resulting in a negative A. In order to facilitate discussion, the deposition section is erased from the figure. From the spatial aspect, with the increase of the distance from the onset point, A initially increases, then reaches its maximum value near the downstream edge of the dam crest, and finally decreases to zero in the position to which the headcut retrogrades. From the temporal aspect, with elapsed time, various curves of A illustrate that the maximum values of the curves at the downstream edge generally decrease but the values at the upstream and downstream parts of the edge become larger than before. Therefore, the shapes of the curves become podgy over time. In fact, the position of the maximum value is exactly the onset point from which the headcut begins. Due to the large energy slope of the edge on the inner slope, the overflow starts to scour the sediment material as it flows through the initial breach. Hence, the headcut erosion increases to a high value, and then decreases moderately because of the headcut migration leading to a gentle slope. Conversely, in the positions far from the onset point, the values of A rise gradually from small ones when the flow condition strengthens and the headcut develops upstream, resulting in a relatively high energy slope with respect to a fixed section.

After the first two stages, the dam crest elevation started to decrease and the sliding failure occurred due to the intensely vertical erosion. Three typical control cross-sections were selected to study the characteristics of the vertical erosion rate along the dam profile. The three cross-sections with distances of 10 cm, 65 cm, and 105 cm from the original section

represented the upstream, middle, and downstream regions of the dam, respectively (Fig. 1).

Fig. 5 shows the variation of the vertical erosion rate at the three control cross-sections during the dam break process for run 7. At the first two stages, the erosion rate of the upstream region where the erosion is going to develop is zero at first, then gradually increases due to the headcut migration; the erosion rate of the middle region where the erosion starts is significantly larger than zero due to the large energy slope; and the erosion rate of the downstream region where the sediment is deposited is negative, because the erosion rate cannot neutralize the deposition rate.
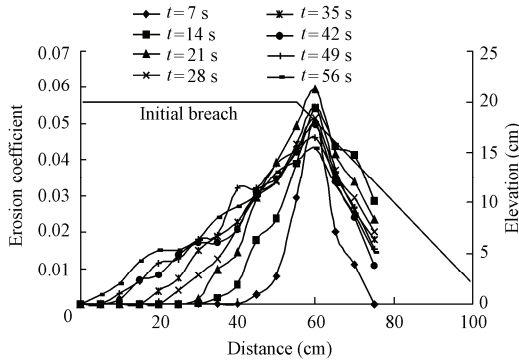

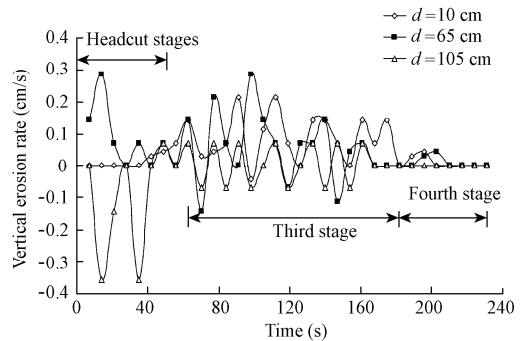Fig. 4 Varied erosion coefficient A for run 7 at different time

Fig. 5 Different vertical erosion rates in three regions of dam for run 7

At the third stage, the vertical erosion rate of the three regions has some common aspects. First, the vertical erosion rate curves fluctuate with a large amplitude. Owing to the intense vertical erosion, the horizontal erosion in the form of a sliding failure occurs frequently, and the eroded sediment falls onto the breach, reducing the energy slope of the overflow temporarily. Hence, the vertical erosion rate decreases immediately. After the sediment sliding from the dam crest is transported downstream, the vertical erosion rate increases again rapidly. Second, the vertical erosion rates of the three regions generally reach their maximum values at this stage. In addition, the horizontal erosion mostly occurs in this stage. Therefore, it can be concluded that the erosion rate is most intense in the third stage.

At the fourth stage, the vertical erosion ends, and the vertical erosion rate reaches zero.

3.2 Sediment transport

The sediment transport process of the dam break, which is non-uniform and unsaturated, cannot be calculated by conventional formulas established for uniform sediment transport. With the dam deformation monitored in vertical and horizontal directions, the sediment transport rate was obtained during the dam break process. In this study, the impacts of the length of the dam crest, the inner slope, and the dam composition on the sediment transport rate of dam break resulting from overtopping were examined.

The relationships between the sediment transport rate and elapsed time with lengths of

the dam crest of 10 cm, 20 cm, and 25 cm, are plotted in Fig. 6 (the dam was constructed with Sediment C at an inner slope of 21.81°). For a given length, the sediment transport rate gradually increases due to the headcut, then reaches its peak value at the third stage, and finally decreases to zero. The reasons may be as follows: during the headcut migration, the sediment transport rate is small due to the little discharge of overflow at a small velocity. In the third stage, a large amount of overflow with a high velocity can entrain a large amount of sediment. As the breach grows, the reservoir elevation drops and the potential energy is released. Therefore, the sediment transport rate decreases continually to zero.

It is found that for the longer dam crest, the peak sediment transport rate is lower than that of the shorter one. The length of the dam crest also affects the arrival time of the peak sediment transport rate: a longer dam crest takes more time to obtain the peak sediment transport rate than a shorter one.

Fig. 7 shows the sediment transport rate curve and discharge curve for run 1. Through comparison of the two curves, it can be seen that the peak sediment transport rate is reached before the peak discharge. The same phenomenon can be found in other runs. The reasons may be as follows: in the third stage, as the breach is degraded for vertical erosion, the sidewall becomes steeper and finally falls onto the channel, blocking the upstream overflow. When the deposit is transported downstream, the sediment transport rate rapidly increases to its maximum value. Meanwhile, the breach is broadening due to the sediment transport. After the deposit is washed out totally, the peak discharge arrives because of the larger flow cross-section area. It can be concluded that the overflow discharge relies on the sediment transport during the breaching process.
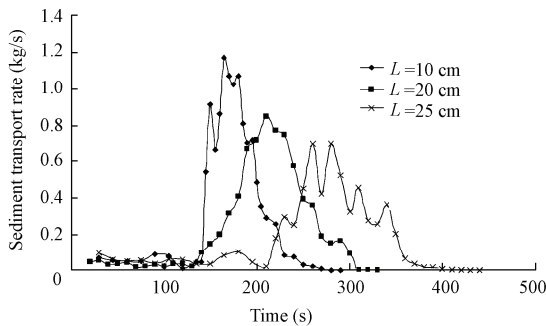

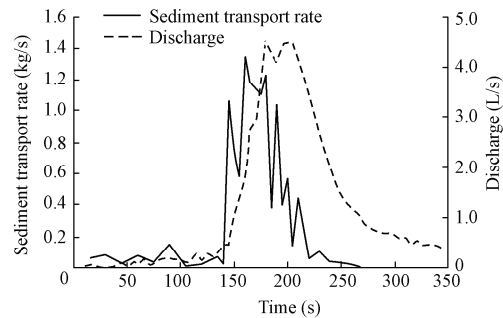**Fig. 6** Sediment transport rate for different dam crest lengths

Fig. 7 Comparison of sediment transport rate and discharge curves for run 1

A relationship between the peak sediment transport rate and the length of the dam crest, shown below, can be obtained with experimental data through regression analysis (Fig. 8):

$$g_{max} \sim 4.12 L^{0.54} \tag{2}$$

where g_{max} is the peak sediment transport rate for the dam break progress (kg/s).

The relationships between the sediment transport rate and elapsed time on inner slopes of

21.81°, 26.58°, 18.44°, and 14.04° are plotted in Fig. 9 (the dam with a length of 20 cm was constructed with Sediment C). For a given inner slope, the same trend as above can be found: the sediment transport rate initially increases, and then arrives at its maximum value, and finally decreases.
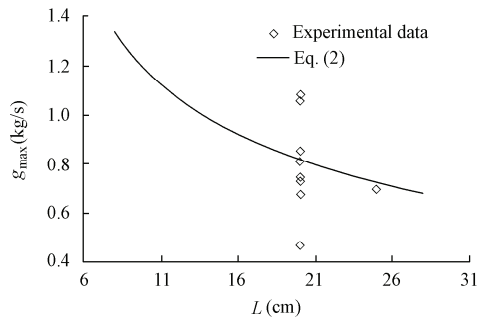

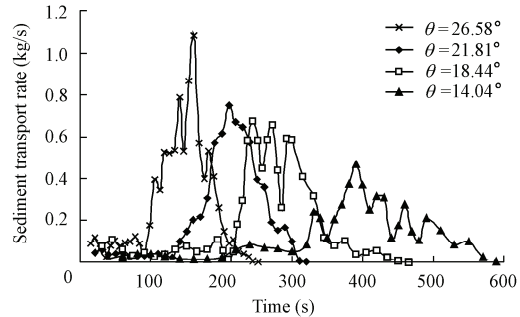**Fig. 8** Peak sediment transport rate versus length of dam crest

Fig. 9 Sediment transport rate for different inner slopes

The inner slope of the dam affects both the value and the arrival time of the peak sediment transport rate: a flatter inner slope takes longer to obtain the peak sediment transport rate than the steeper one and obtains a smaller peak sediment transport rate. Similarly, the relationship between the peak sediment transport rate and the inner slope can be obtained using the experimental data and is exhibited by Eq. (3), as well as Fig. 10.

$$g_{max} \sim 2.33(\tan\theta)^{1.16} \tag{3}$$

The relationships between the sediment transport rate and elapsed time with various dam compositions represented by different non-uniformity coefficients, i.e. $S = 2.25$, 2.3, 3.14, and 3.21, are plotted in Fig. 11 (the dam with a length of 20 cm was constructed at an inner slope of 21.81°). For a given S, the same trend as above of the sediment transport rate varying with elapsed time can be found. However, with the increase of S, the peak sediment transport rate initially increases, and then decreases. The reasons may be as follows: S increases with the number of coarse grains in dam materials. However, the majority of transported sediment is fine grains because the coarse grains move sporadically during the dam break processes. At first, the proportion of coarse grains is small so that they are distributed far from one another on the bed surface of the dam. Considering the fact that coarse grains can emerge in the shallow flow, the coarse grains reduce the efficient flow cross-section area, increase the flow velocity, and disturb the flow regime. Consequently, more fine grains are transported and the peak sediment transport rate increases. As the proportion of coarse grains becomes larger, the relative exposure degree coefficient (Han 1999) increases significantly for a considerable growth rate of the median grain in the bed surface. Hence, the equivalent grain sizes (Liu 2004) of the sediment increase, and higher incipient velocities are required. As a result, fewer fine grains are transported and the peak sediment transport rate decreases.
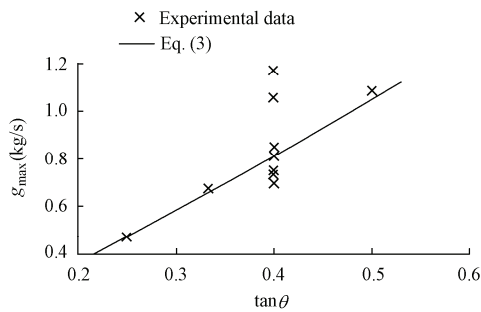
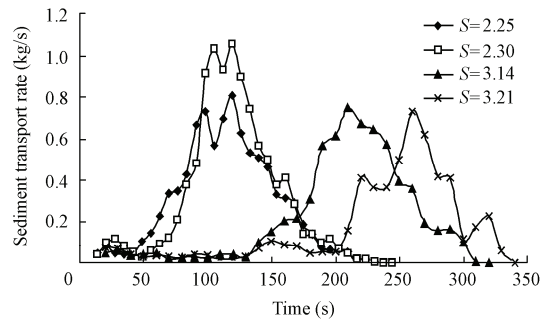**Fig. 10** Peak sediment transport rate versus tanθ

Fig. 11 Sediment transport rates for different inner slopes

Fig. 12 represents the relationship between g_{max} and S using the experimental data. It shows that the peak sediment transport rate is the exponent function of the non-uniformity coefficient, rather than the power function of that:

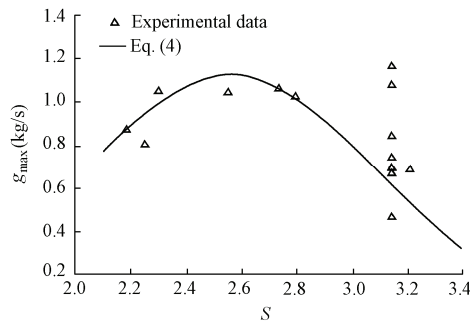$$g_{max} \sim e^{-1.794S^2 + 9.185S - 11.638} \tag{4}$$

Fig. 12 Peak sediment transport rate versus non-uniformity coefficient S

4 Conclusions

This paper presents new experimental data of the erosion rate and the sediment transport rate during the dam break processes via 13 flume experiments. The dam break was assumed to occur due to overtopping with an initial breach. The dam material was composed of non-cohesive sand whose median diameter was larger than 1 mm.

During the first two stages, the dam went through the headcut erosion until the dam crest vanished. Using the equation proposed by Begin et al. (1980), the erosion coefficient of the headcut was calculated. The main conclusions are as follows: the maximum value of erosion coefficient A always occurs near the downstream edge of the dam crest, and, with the elapsed time, the curve shape of the erosion coefficient becomes podgy.

The characteristics of the vertical erosion rate along the dam profile were studied by dividing the dam into three regions. The main conclusions are as follows: when the headcut starts to migrate, the vertical erosion rate for the middle region of the dam is positive, whereas the rate for the downstream region is negative. No erosion is observed in the upstream region

of the dam till the headcut regresses to this region. The whole dam suffers most intense erosion in the third stage.

Three relevant parameters affecting sediment transport during the dam breakage processes were discussed in this paper: the length of the dam crest, the inner slope, and the dam composition. It can be found that a longer dam crest and flatter inner slope reduce the maximum sediment transport rate, and prolong the arrival time of the peak value. However, with the increase of the non-uniformity coefficient S, the peak sediment transport rate initially increases, and then decreases. The conclusions can provide references for safety assessment and reinforcement of blocked dams caused by geo-hazards.

References

Begin, Z. B., Schumm, S. A., and Meyer, D. F. 1980. Knickpoint migration due to baselevel lowering. *Journal of the Waterway, Port, Coastal and Ocean Division*, 106(3), 369-389.

Chen, L. K., and Chen, S. C. 2006. Retrogressive erosion and longitudinal profile evolution in noncohesive material. *International Journal of Sediment Research*, 21(2), 113-122.

Chinnarasri, C., Tingsanchali, T., Weesakul, S., and Wongwises, S. 2003. Flow patterns and damage of dike overtopping. *International Journal of Sediment Research*, 18(4), 301-309.

Clayton, J. A., and Knox, J. C. 2008. Catastrophic flooding from Glacial Lake Wisconsin. *Geomorphology*, 93(3-4), 384-397. [doi:10.1016/j.geomorph.2007.03.006]

Dai, F. C., Lee, C. F., Deng, J. H., and Tham, L. G. 2005. The 1786 earthquake-triggered landslide dam and subsequent dam-break flood on the Dadu River, southwestern China. *Geomorphology*, 65(3-4), 205-221. [doi:10.1016/j.geomorph.2004.08.011]

Dodge, R. A. 1988. *Overtopping Flow on Low Embankment Dams: Summary Report of Model Tests*. Denver: U.S. Department of the Interior, Bureau of Reclamation.

Dong, J. J., Tung, Y. H., Chen, C. C., Liao, J. J., and Pan, Y. W. 2011. Logistic regression model for predicting the failure probability of a landslide dam. *Engineering Geology*, 117(1-2), 52-61. [doi:10.1016/j.enggeo.2010.10.004]

Dumbser, M. 2011. A simple two-phase method for the simulation of complex free surface flows. *Computer Methods in Applied Mechanics and Engineering*, 200(9-12), 1204-1219. [doi:10.1016/j.cma.2010.10.011]

Han, Q. W., and He, W. M. 1999. *The Incipient Mechanism and Velocity of Sediment*. Beijing: Science Press. (in Chinese)

Li, M. H., Sung, R. T., Dong, J. J., Lee, C. T., and Chen, C. C. 2011. The formation and breaching of a short-lived landslide dam at Hsiaolin Village, Taiwan, part II: Simulation of debris flow with landslide dam breach. *Engineering Geology*, 123(1-2), 60-71. [doi:10.1016/j.enggeo.2011.05.002]

Li, T. C., Schuster, R. L., and Wu, J. S. 1986. Landslide dams in south-central China. *Landslide Dam: Processes, Risk, and Mitigation*, 146-162. New York: American Society of Civil Engineers.

Li, Y., and Li, J. 2009. Review of experimental study on dam-break. *Advances in Water Science*, 20(2), 304-310. (in Chinese)

Liu, X. N. 2004. *Gravel Bed-load Transport and its Modelling*. Ph. D. Dissertation. Chengdu: Sichuan University. (in Chinese)

Marzolff, I., and Poesen, J. 2009. The potential of 3D gully monitoring with GIS using high-resolution aerial photography and a digital photogrammetry system. *Geomorphology*, 111(1-2), 48-60. [doi:10.1016/j.geomorph.2008.05.047]

Menéndez-Duarte, R., Marquínez, J., Fernandez-Menéndez, S., and Santos, R. 2007. Incised channels and gully erosion in Northern Iberian Peninsula: Controls and geomorphic setting. *Catena*, 71(2), 267-278. [doi:10.1016/j.catena.2007.01.002]

Ralston, D. C. 1987. Mechanics of embankment erosion during overflow. Ragan, R. M., ed., *Proceedings of*

the 1987 National Conference on Hydraulic Engineering, 733-738. New York: American Society of Civil Engineers.

Schuster, R. L., and Costa, J. E. 1986. A perspective on landslide dams. Schuster, R. L., ed., *Landslide Dam: Processes, Risk, and Mitigation*, 1-20. New York: American Society of Civil Engineers.

Stavi, I., Perevolotsky, A., and Avni, Y. 2010. Effects of gully formation and headcut retreat on primary production in an arid rangeland: Natural desertification in action. *Journal of Arid Environments*, 74(2), 221-228. [doi:10.1016/j.jaridenv.2009.08.007]

Visser, P. J. 1998. *Breach Growth in Sand-dikes*. Ph. D. Dissertation. Delft: Delft University of Technology.

Wahl, T. L. 1998. *Prediction of Embankment Dam Breach Parameters: A Literature Review and Needs Assessment*. Denver: U.S. Department of the Interior, Bureau of Reclamation.

Yan, J., Cao, Z. X., Liu, H. H., and Chen, L. 2009. Experimental study of landslide dam-break flood over erodible bed in open channels. *Journal of Hydrodynamics*, Ser. B, 21(1), 124-130. [doi:10.1016/S1001-6058(08)60127-4]

Zhang, J., Cao, S. Y., Yang, F. G., Luo, L. H., and Huang, E. 2010. Experimental study on outlet and scour of blocked dam. *Journal of Sichuan University (Engineering Science Edition)*, 42(5), 191-196. (in Chinese)

Zhu, Y. H. 2006. *Breach Growth in Clay-dikes*. Ph. D. Dissertation. Delft: Delft University of Technology.

(Edited by Yan LEI)